Supporting Information

Leroy et al. 10.1073/pnas.1412389112

SI Materials and Methods

Subjects. We studied the following typical groups of infants, right-handed children, and adults:

- 14 healthy full-term infants (mean age = 11.1 ± 3.9 wk; nine males, five females) imaged in Necker Hospital (Assistance-Publique Hôpitaux de Paris, France). These data have been published already (1).
- 18 right-handed boys (mean age = 10.6 ± 1.3 y) from the Kennedy Krieger Institute selected as control subjects in the ABIDE project (2). Note that one subject appeared as an outlier in our analyses. He had a strong asymmetry in the STAP but in the opposite direction (see the orange dot in the lower left quadrant in Fig. S2*A*). We checked the MRI data carefully and found that this subject also had a reverse pattern of petalia, suggesting that the MR image might have been flipped accidentally. However, because we could not prove the MRI flipping, this subject was included in all analyses. When this subject is excluded, boys have a STAP amplitude similar to that of girls (boys: AI = 21 ± 14%; girls: AI = 24 ± 23%; $P = 0.7$; Welch t test), and the STAP amplitude is +22% in children, not +19% as shown in Table 1.
- 10 right-handed girls (mean age = 9.6 ± 0.4 y) imaged at the NeuroSpin center (CEA, Gif sur Yvette, France). Written informed consent was obtained from their parents. The protocol was approved by the ethical committee. We used these subjects as controls for studying the effect of AgCC on STS asymmetry.
- 47 young right-handed adults (mean age = 21 ± 1.2 y; 23 females, 24 males) imaged at the NeuroSpin center (CEA, Gif sur Yvette, France). The protocol was approved by the ethical committee.

We studied the following atypical human groups of left-handed adults with left- and right-hemispheric language dominance (LLg and RLg, respectively), children with autism spectrum disorders (ASD), children with AgCC, adults with situs inversus, and adults with Turner syndrome. We also included a group of chimpanzees:

- 48 young left-handed adults from Van der Haegen's study (3), consisting of 14 males (mean age = 22 ± 4 y), 17 LLg adult females (mean age = 20 ± 1.6 y) and 17 RLg adult females (mean age = 20.2 ± 1.5 y). Only female subjects with a strong hemispheric dominance (lateralization index smaller than −0.6 or greater than 0.6) were included in this study. See Van der Haegen et al. (4) for further details on subject recruitment and protocol approval.
- 15 autistic right-handed boys (mean age = 10.0 ± 1.5 y) from the Kennedy Krieger Institute through the ABIDE project. Handedness, intelligence assessment tests, and psychiatric diagnoses can be found on the ABIDE Website (2). The ABIDE database is open for data sharing in the scientific community.
- 5 right-handed girls with a prenatal diagnosis of isolated corpus callosum dysgenesis (mean age = 11.4 ± 1.5 y) imaged at the NeuroSpin center (CEA, Gif sur Yvette, France). Three children presented with complete AgCC; two children had a partial corpus callosum agenesis restricted to the genu. Thus, the amount of callosal fibers along the STS is assumed to be strongly reduced in every child (5). All had normal psychomotor development, clinical evaluation, and Intellectual Quotient. Written informed consent was obtained from their parents. The protocol was approved by the ethical committee (CCP Kremlin Bicêtre) (6).
- 6 adults with situs inversus from the Situs Inversus Project managed by N.R. Three of these subjects—one 49-y-old right-handed woman and two 33-y-old right-handed men—have been studied by Kennedy et al. (7). All three had reversed petalia and left hemispheric language dominance. Two other subjects, a 46-y-old right-handed man and an 81-y-old left-handed man, have been studied by Ihara et al. (8). Both had reversed petalia and RLg. The last subject was a 43-y-old right-handed Taiwanese man with a score of 100 on the Edinburgh Handedness Inventory (9). MR images were acquired at the National Yang-Ming University, Taipei City, Taiwan. He had normal general health with no history of developmental defects of the cardiopulmonary system, learning disorders, neurologic disorders, or psychiatric disease. We manually assessed the reverse pattern of petalia: The left frontal lobe was shifted anteriorly with respect to the right, and the right occipital lobe was shifted posteriorly with respect to the left. His hemispheric language dominance was not investigated.
- 14 patients with Turner syndrome (mean age = 24.5 ± 6 y) from Molko's study (10) imaged at the Frederic Joliot Hospital (CEA, Orsay, France). All had the main features of the Turner syndrome phenotype. Ten were of the 45,X karyotype, and four showed a mosaic. See Molko et al. (10) for further details on subject recruitment and protocol approval.
- 73 adult chimpanzees (47 females, 26 males; mean age = 23 y ± 12 y) from the Division of Developmental and Cognitive Neuroscience at the Yerkes National Primate Research Center, Atlanta, GA. See ref. 11 for further details on subjects and study approval.

MRI Acquisition Parameters. Parameters are given in Table S1.

Data Processing. ***Brain segmentation and sulci detection.*** We applied the BrainVISA Morphologist pipeline procedure* (12, 13) on all datasets except infants. The pipeline process consists of segmenting the brain and extracting the sulci from the gray–white-matter interface. It includes the following steps: correction for spatial inhomogeneities in the T1w signal intensity, splitting of the hemispheres, tissue statistics estimation, white–gray matter classification, cortical reconstruction, normalization toward the Talairach space, and sulcal detection and recognition. It runs automatically as soon as both anterior and posterior brain commissures have been specified manually on the MRI. A quality check was performed on each subject.

In patients with Turner syndrome, the same procedure was followed, but the normalization step based on the Statistical Parametric Mapping software (SPM99); only the normalized data were accessible; the raw images were not (14). Distance errors of anatomical landmarks across subjects have been shown to be slightly reduced with SPM-type normalization compared with the linear transformation that we used in this study (15). Furthermore, the MNI coordinates provided with SPM can be converted easily to the Talairach coordinates of our study with errors less than 5 mm (imaging.mrc-cbu.cam.ac.uk/imaging/MniTalairach). Thus, we believe that this normalization process has only a minor impact on both the magnitude and spatial extent of the STS asymmetry.

To account for the differences in chimpanzee brains, a number of adjustments were necessary to take into account the different

*Fischer C, The 18th Annual Meeting of the Organization for Human Brain Mapping, June 10–14, 2012, Beijing, China.

structural characteristics of the two species (11). Chimpanzee MRI scans first were skull-stripped, cropped, and reformatted at 0.7-mm cubic isotropic resolution using Analyze 8.1 (BIR, Mayo Clinic) software. Adjustments sometimes were needed in estimating tissue statistics to distinguish gray and white matter better in chimpanzee brain scans. Manual correction of the split-brain mask sometimes was needed to label hemispheres and cerebellum properly. Finally, the size of the morphological closing of the hemispheric segmentation was set to 5 mm as opposed to 10 mm in human children and adults.

In infants, brain was segmented on T2w MR images, which provide better white–gray matter contrast than T1w images at this age using a dedicated approach (16). Normalization was a two-steps process. Brains first were normalized toward a common infant template by using the left and right brain surface envelope (1). Then, the infant template was linearly normalized to the Talairach space using a common scaling factor of 1.4 in all three dimensions [see supplementary materials in Dehaene-Lambertz et al. (17)].

STS identification. We identified the STS in each subject. In chimpanzees, it is a long and linear sulcus with very few branches, which runs below the sylvian fissure from the temporal pole to the inferior parietal lobule. In infants, the sulcation also was rather straightforward: We found only two full sulcal interruptions (on two left hemispheres), and there was only one caudal branch connected to the main sulcal part. Because automatic sulcus delineation remains an open issue during the first postnatal months (1), the sulcus was drawn manually in the MR images using the Anatomist software (18). The drawing was blinded both to infant age and to the side convention of the acquisitions. It was managed slice by slice, starting from the outer section of the brain and moving inward until a wall of gray matter was met (1).

In children and adults, the STS shape often is segmented and bent in places. In the temporal pole, there is a small sulcus below the superior temporal plane, which most often is disconnected from the STS, usually being shallow and either running inwardly toward medial regions or having a different orientation from the STS. This sulcus was not included in our definition of the STS. See *Sulcal interruptions* for our handling of other sulcal interruptions. Of note, a few sulci (7% in children; 17 % in right-handed adults) had an unusual connection to the sylvian fissure, all of which occurred in the left hemispheres. In these cases, definition of the STS stopped where the sulcus connected to the sylvian fissure.

In most human brains, the identification of STS caudal branches presents a major issue. Across all human subjects in this study (except infants), only one STS (in a subject with situs inversus) had only a single caudal branch. In the majority of hemispheres we found three caudal branches, i.e., anterior, central, and posterior (19); in the remaining hemispheres, we found only anterior and posterior branches. In all cases we excluded the posterior branch, which often is horizontal and more ventral than the other branches and is unlikely to be part of the angular gyrus. We selected the anterior branch in subjects having only two caudal branches in a given hemisphere (children: 61%; children with ASD: 40%; right-handed females: 48%; right-handed males: 58%; LLg females: 41%; RLg females: 71%; left-handed males: 62%). In the contralateral hemisphere, we selected the caudal branch (the anterior branch or the central branch) whose location was the most symmetrical in relation to the interhemispheric plane. In a few cases, these branches were equidistant from the contralateral branch, so we added another criterion: Because left caudal branches usually are more posterior than right ones (19), we selected the anterior (central) branch for right (left) hemispheres, respectively.

For the remaining human subjects, who had three caudal branches in both hemispheres, the location of the angular gyrus was not easily determined because most modern atlases consider only two caudal branches (20, 21). Furthermore, there are discrepancies between atlases, which locate the angular gyrus at the termination of either the anterior branch or the central branch (19). Therefore we used a developmental approach and selected the branch that most deeply joined with the main temporal part of the STS, i.e., a true connection as described in Ono's atlas (20). Indeed, the posterior part of the STS often is continuous up to the angular gyrus in infant brains (1), and the deepest parts of sulci form early and retain their identity during development in several species (22, 23). Using this approach, we selected either a pair of left–right anterior branches or a pair of left–right central branches for each subject (percent of central branches in normally developing children: 64%; in children with ASD: 44%; in right-handed females: 73%; in right-handed males: 70%; in LLg females: 40%; in RLg females: 60%; in left-handed males: 67%).

Note that caudal branches were posterior to the asymmetrical segment that we describe here. As reported in this paper, the STAP region terminates 10 mm posterior to the planum landmark in typical subjects. We measured the distance (d_{caudal}) between the planum landmark and the most anterior part of caudal branches along the coronal axis. Most branches started posteriorly to the STAP region (d_{caudal} >10 mm). The percentage of subjects with d_{caudal} >10 mm in infants was 100% on the left, 57% on the right; in children: 93% on the left, 86% on the right; in right-handed adults: 91% on the left, 77% on the right. Thus, our choice of caudal branches had little effect, if any, on the STAP magnitude in these groups.

The planum temporale as sulcal landmark. To set the origin of sulcal depth profile, we defined a common landmark in all subjects. As in Glasel et al. (1), we chose the deepest location of the planum temporale, which is located in the posterior part of the insula posterior to the medial tip of Heschl's gyrus. This location has been shown to be relatively stable across subjects (1). In cases where Heschl's gyrus was duplicated, the landmark was set posterior to the most anterior transverse gyrus according to a common definition of the anterior border of the planum temporale (24). We then projected the planum landmark onto the STS along the dorso–ventral axis to set the profile origin (Fig. S1 *C–E*). Depth profiles both within and across groups of subjects were aligned according to the sulcal coordinates origin.

Note that the left landmark is slightly more posterior than the right along the coronal axis in all groups (with $\Delta = |y_{left} - y_{right}|$ in Talairach space, infants: $\Delta = 4.2 \pm 8$ mm, $P = 0.06$; children: $\Delta = 3.1 \pm 3$ mm, $P < 0.001$; children with ASD: $\Delta = 5.0 \pm 4$ mm, $P < 0.001$; right-handed adults: $\Delta = 3.7 \pm 3$ mm, $P < 0.001$; left-handed adults: $\Delta = 1.2 \pm 3$ mm, $P = 0.006$; chimpanzees: $\Delta = 1.2 \pm 2$ mm, $P < 0.001$). However, this right–left landmark difference based on an anatomical landmark provides an overall better alignment of the left and right depth profiles than the choice of homologous image coordinates in both hemispheres.

Location and extent of the STAP. We computed the overlap of group-specific asymmetrical segments in the sulcal coordinate systems across typically developing groups, i.e., infants, right-handed children, and adults (anterior border: $x = -35$ mm; center: $x = -12$ mm; posterior border: $x = +10$ mm along the sulcus). This overlap constituted the STAP. The location of the STAP then was computed in the Talairach referential for each hemisphere and averaged across subjects. Profiles from both children and adults were used for computing mean Talairach coordinates; infants' profiles were omitted because of the sulcal parameterization used (1) and because the normalization process (see *Data Processing*) might be less accurate in infants than in children and adults.

Sulcal interruptions. We assessed how anatomical interruptions of the sulcus might influence overall STS asymmetry. Sulcal interruptions (*plis de passage*) might signal enhanced connectivity between adjacent gyri and have been used by anatomists to characterize primate brains (25).

We detected sulcal interruptions in every subject. Interruptions can either be full or partial. A full interruption occurs when the sulcus is broken into two pieces, e.g., when a transverse gyrus

connects the superior temporal gyrus with the middle temporal one. In most cases, contiguous sulcal parts simply were concatenated to get one continuous morphological structure. In the case of parallel parts, however, we kept only the sulcal part closest to the superior temporal gyrus. For example, in Fig. S1 the sulcal tip "s2" is closer to the gyrus than the sulcal tip "s3," so that sulcal parts are concatenated by projecting tip "s2" on the other part of the sulcus. In contrast, a sulcal interruption is partial when the transverse gyrus is buried in the depth of the sulcus, causing only a local elevation of the sulcus floor, a *pli de passage* (26). (We have used "*pli de passage*" as generic name for sulcal interruptions, because a full interruption can be seen as a superficial *pli de passage*.)

Because sulcal interruptions could affect the depth of the sulcus, we ran a post hoc analysis to assess their effect on depth asymmetry. We computed the occurrence and size of *plis de passage* in each group over the STAP. Interruptions were characterized by local minima along the depth profile. They were detected if they were at least 5 mm lower than neighboring local maxima. This threshold was chosen empirically to minimize the false detection rate caused by several sources of noise, e.g., partial volume effects close to the cortical–pial interface in the MR image and inaccuracies in brain segmentation and in sulcal parameterization. Furthermore, because the spatial extent of interruptions is a few millimeters wide, interruptions were considered when they were less than 5 mm away from the STAP, i.e., in the sulcal range of −40, +15 mm. Because it has been shown in adults that *plis de passage* occur more often on the left STS than on the right (27), we tested this hypothesis in each group using Fisher's exact test (Table 1). Eventually we estimated the interruption size over the depth profiles as the depth gap between the local minimum that defined the *pli de passage* and nearby local maxima on both sides of this minimum (Fig. S1).

We assessed whether asymmetrical sulcal interruptions might explain STS depth asymmetry. Accordingly, all human subjects were divided into two groups: the *pli de passage* (PP) group, which included 100 subjects having an interruption in one or the other hemisphere within the STAP, and the no *pli de passage* (noPP) group containing 77 subjects with continuous sulci in both hemispheres.

As expected in the PP group, the left–right difference in interruption size is correlated with the STAP ($R^2 = 0.45$; $P < 0.001$) (Fig. S2*A*). The increase of the STAP in the PP group compared with the noPP group also was seen when analysis was restricted to the typical groups (PP AI = 33% ± 33% > noPP AI = 16% ± 11%; PP–noPP factor: $F_{1,85} = 11.5$; $P = 0.001$; infant–child–adult factor: $F_{2,85} = 2.1$; $P = 0.1$; two-way ANOVA).

In the noPP group, the STAP remained significant in 97% of subjects without *plis de passage* (Fig. S2*B*): infants: $P < 0.001$; children: $P < 0.001$; children with ASD: $P = 0.004$; children with AgCC: $P = 0.2$; left-handed adult LLg females: $P = 0.002$; left-handed adult RLg females: $P = 0.002$; left-handed male adults: $P = 0.06$; right-handed female adults: $P < 0.001$; right-handed male adults: $P < 0.001$; adults with situs inversus: $P = 0.004$; adults with Turner syndrome: $P = 0.03$.

1. Glasel H, et al. (2011) A robust cerebral asymmetry in the infant brain: The rightward superior temporal sulcus. *Neuroimage* 58(3):716–723.
2. Autism Brain Imaging Data Exchange (ABIDE) project (2010) Available at fcon_1000.projects.nitrc.org/indi/abide. Accessed October 2012.
3. Van der Haegen L, Cai Q, Brysbaert M (2012) Colateralization of Broca's area and the visual word form area in left-handers: fMRI evidence. *Brain Lang* 122(3):171–178.
4. Van der Haegen L, Cai Q, Seurinck R, Brysbaert M (2011) Further fMRI validation of the visual half field technique as an indicator of language laterality: A large-group analysis. *Neuropsychologia* 49(10):2879–2888.
5. Witelson SF (1989) Hand and sex differences in the isthmus and genu of the human corpus callosum. A postmortem morphological study. *Brain* 112(Pt 3):799–835.
6. Bénézit A, et al. (2015) Organising white matter in a brain without corpus callosum fibres. *Cortex* 63:155–171.
7. Kennedy DN, et al. (1999) Structural and functional brain asymmetries in human situs inversus totalis. *Neurology* 53(6):1260–1265.
8. Ihara A, et al. (2010) Neuroimaging study on brain asymmetries in situs inversus totalis. *J Neurol Sci* 288(1-2):72–78.
9. Oldfield RC (1971) The assessment and analysis of handedness: The Edinburgh inventory. *Neuropsychologia* 9(1):97–113.
10. Molko N, et al. (2004) Brain anatomy in Turner syndrome: Evidence for impaired social and spatial-numerical networks. *Cereb Cortex* 14(8):840–850.
11. Bogart SL, et al. (2012) Cortical sulci asymmetries in chimpanzees and macaques: A new look at an old idea. *Neuroimage* 61(3):533–541.
12. Perrot M, Rivière D, Mangin JF (2011) Cortical sulci recognition and spatial normalization. *Med Image Anal* 15(4):529–550.
13. Mangin JF, et al. (2004) Object-based morphometry of the cerebral cortex. *IEEE Trans Med Imaging* 23(8):968–982.
14. Ashburner J, Friston KJ (2000) Voxel-based morphometry—the methods. *Neuroimage* 11(6 Pt 1):805–821.
15. Klein A, et al. (2009) Evaluation of 14 nonlinear deformation algorithms applied to human brain MRI registration. *Neuroimage* 46(3):786–802.
16. Leroy F, et al. (2011) Atlas-free surface reconstruction of the cortical grey-white interface in infants. *PLoS ONE* 6(11):e27128.
17. Dehaene-Lambertz G, Dehaene S, Hertz-Pannier L (2002) Functional neuroimaging of speech perception in infants. *Science* 298(5600):2013–2015.
18. Cointepas Y, Mangin JF, Garnero L, Poline JB, Benali H (2001) BrainVISA: Software platform for analysis of multi-modality brain data. *Neuroimage* 13(6):S98.
19. Segal E, Petrides M (2012) The morphology and variability of the caudal rami of the superior temporal sulcus. *Eur J Neurosci* 36(1):2035–2053.
20. Ono M, Kubik S, Abernathey C (1990) *Atlas of the Cerebral Sulci* (Thieme Medical Publishers, Inc., New York).
21. Duvernoy H (1999) *The Human Brain: Surface, Blood Supply and Three-Dimensional Sectional Anatomy* (Springer Wien, New York).
22. Welker W (1990) Why does cerebral cortex fissure and fold? *Cerebral Cortex* 8(B):3–136.
23. Smart IH, McSherry GM (1986) Gyrus formation in the cerebral cortex in the ferret. I. Description of the external changes. *J Anat* 146:141–152.
24. Galaburda AM, Corsiglia J, Rosen GD, Sherman GF (1987) Planum temporale asymmetry, reappraisal since Geschwind and Levitsky. *Neuropsychologia* 25(6):853–868.
25. Gratiolet P (1854) *Mémoires sur les Plis Cérébraux de l'Homme et des Primates* (Bertrand Arthus, Paris).
26. Régis J, et al. (2005) "Sulcal root" generic model: A hypothesis to overcome the variability of the human cortex folding patterns. *Neurol Med Chir (Tokyo)* 45(1):1–17.
27. Ochiai T, et al. (2004) Sulcal pattern and morphology of the superior temporal sulcus. *Neuroimage* 22(2):706–719.

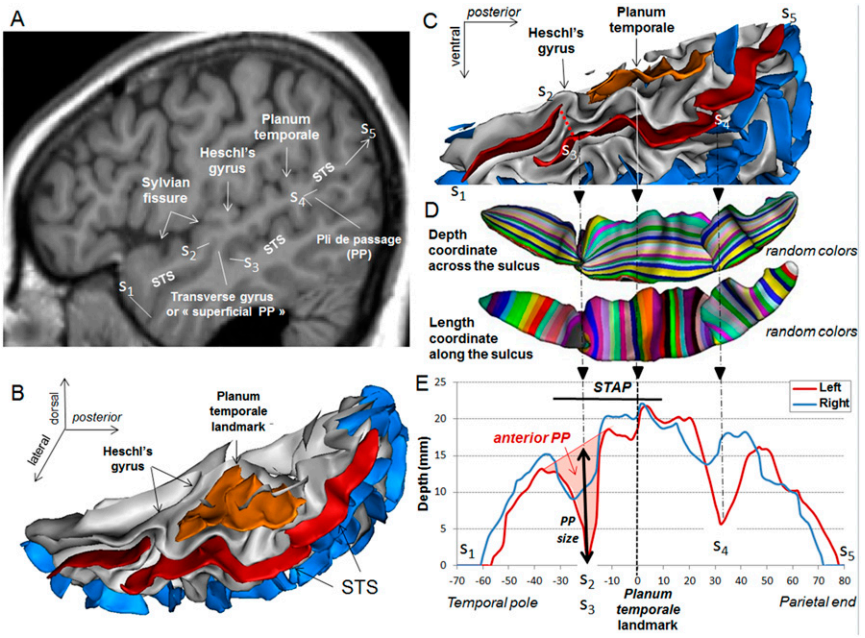

Fig. S1. Computation of the STS depth profile in a left sulcus with two *plis de passage*: one superficial *pli de passage* (i.e., a full interruption) at the STAP and a buried *pli de passage* posterior to the planum landmark (partial interruption). (*A*) MRI of an adult subject with left STS in three parts: from s_1 to s_2, from s_3 to s_4, and from s_4 to s_5. (*B*) The planum temporale landmark is located at the most internal tip of the planum (orange), immediately posterior to Heschl's gyrus. The STS is shown in red, and the other sulci are shown in blue. (*C*) Sagittal view of the STS (red) with sulcal landmarks (from s_1 to s_5); note that landmark s_3 has been defined arbitrarily so that the delineated STS excludes the transverse gyrus from the superior temporal gyrus. The ventral projection of the planum landmark onto the STS defines the origin of the coordinate system. (*D*) Sulcal parameterization. Two coordinate systems have been defined along and across the sulcus to define sulcal coordinates and depth at every location. Each color longitudinal to the sulcus indicates locations of equal depth; each color transverse to the sulcus indicates locations of equal coordinates. (*E*) Left and right depth profiles in Talairach space. The right profile is deeper than the left one near the STAP. Landmarks s_2 and s_3 overlap because sulcal parts have been concatenated. The two sulcal interruptions make two notches on the left profile. The size of the *pli de passage* over the STAP is computed as the height of the anterior notch (light red). See text for details.

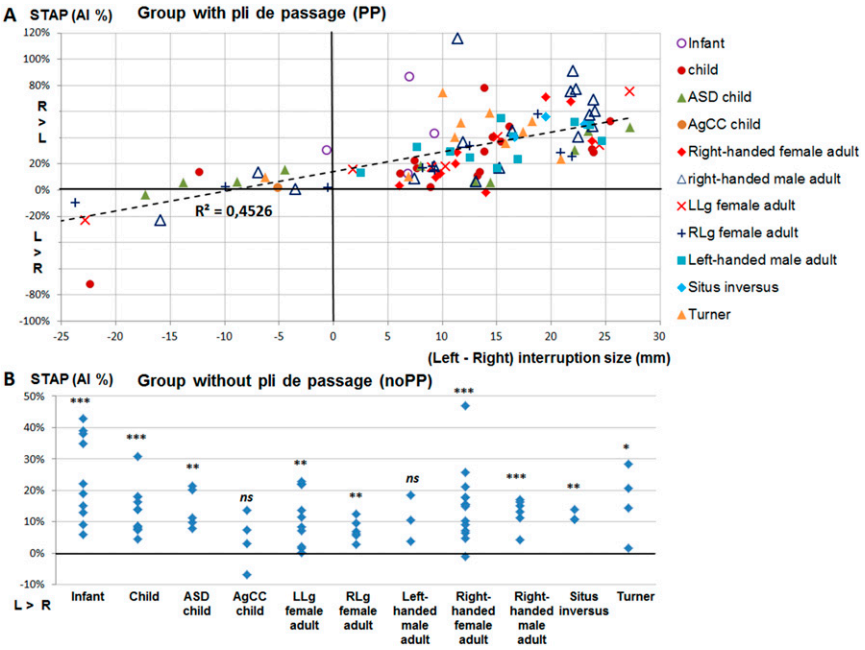

Fig. S2. Relationship between STAP and *plis de passage* in humans. (*A*) Subjects with *pli de passage* over the STAP region (PP group, approximately half of the whole human population). Correlation of the depth asymmetry and the height difference between left and right *plis de passage*. (*B*) Subjects without a *pli de passage* on any hemisphere (noPP group). Despite the lack of sulcal interruption, asymmetrical sulcal depth over the STAP region is present in all groups except children with AgCC and left-handed male adults (small sample sizes). ns, not significant. $*P < 0.05$; $**P < 0.01$; $***P < 0.001$.

Table S1. MRI acquisition parameters

Population	Group	Sex F	Sex M	MRI scanner	Sequence name	TE/TR, ms	No. of signals averaged	Matrix size	Image resolution, mm	Ref.
Infants		5	9	1.5T Signa GE	Axial, sagittal, and coronal fast spin echo	120/5,500	1	192 x 192	0.8 x 0.8 x 2 (in each direction)	(1)
Children	Males		18	3T Achieva Philips	3D MP-RAGE	N.a.	1	256 x 256	1 x 1 x 1	(2)
	ASD males		15							
	Females	10		3T Trio Siemens	3D MP-RAGE	4.18/2,300	1	256 x 256	1 x 1 x 1	(6)
	AgCC females	5								
Right-handed adults		23	24	3T Trio Siemens	3D MP-RAGE	2.98/2,300	1	256 x 240	1 x 1 x 1.1	
Left-handed adults	Males		14	3T Trio Siemens	3D MP-RAGE	2.39/1,550	N.a	256 x 256	0.9 x 0.9 x 0.9	(3)
	LLg females	17								
	RLg females	17								
Situs inversus adults	First set	1	2	1.5 T Signa GE	Coronal inversion recovery SPGR	5/12	1	256 x 192	0.9 x 3 x 0.9	(7)
	Second set	0	2	3T Signa GE	N.a.	N.a.	N.a.	N.a.	1 x 1 x 1	(8)
	Third set	0	1	3T Siemens	3D MP-RAGE	3.5/2,530	1	256 x 256	1 x 1 x 1	
Turner syndrome		14	0	1.5 Signa GE	Axial gradient echo	2.1/10.3	N.a	128 x 128	0.9 x 0.9 x 1.2	(10)
Chimpanzees		47	26	3T Trio Siemens	3D gradient echo	4.4/2,300	3	320 x 320	0.6 x 0.6 x 0.6	(11)

MP-RAGE, magnetization-prepared rapid gradient-echo; n.a., not available; SPGR, spoiled gradient echo.